

Modeling of Photoionized Plasmas

T.R. Kallman

Received: 1 August 2010 / Accepted: 4 November 2010 / Published online: 24 November 2010
© US Government 2010.

Abstract In this paper I review the motivation and current status of modeling of plasmas exposed to strong radiation fields, as it applies to the study of cosmic X-ray sources. This includes some of the astrophysical issues which can be addressed, the ingredients for the models, the current computational tools, the limitations imposed by currently available atomic data, and the validity of some of the standard assumptions. I will also discuss ideas for the future: challenges associated with future missions, opportunities presented by improved computers, and goals for atomic data collection.

Keywords X-ray spectroscopy · Modeling

1 Introduction

The general problem of calculating the reprocessing of ionizing continuum radiation from a star or compact object into longer wavelength lines and diffuse continuum has broad importance in astrophysics. Photoionization modeling is generally thought to include any situation in which the dominant ionization and excitation mechanism is photons from an external source. In addition, key ingredients of such models are applicable more broadly, to calculating the photoelectric opacity and the flux transmitted through any astrophysical gas. In the context of X-ray astronomy, photoionization is important in sources which contain a compact object, notably active galactic nuclei (AGN), X-ray binaries, and cataclysmic variables.

Many of the same principles apply to modeling the properties of diffuse nebulae illuminated by UV radiation from stars, i.e. H II regions and planetary nebulae. Discussions of model line emission from nebulae date from Zanstra (1927), but Seaton and collaborators laid the groundwork for modern numerical modeling by calculating many atomic quantities of importance to nebular modeling (Seaton 1958, 1959; Burgess and Seaton 1960). The subject has been reviewed extensively by Osterbrock and Ferland (2006), and others (see references in Kallman 2001) In this volume, many of the relevant ideas have been discussed

T.R. Kallman (✉)
NASA Goddard Space Flight Center, Greenbelt, MD 20771, USA
e-mail: Timothy.R.Kallman@nasa.gov

by Foster et al. (2010). This paper will not repeat this material, but rather will describe the specific developments modeling of photoionized plasmas which are relevant to X-ray astronomy.

2 What is Photoionization

For the purposes of subsequent discussion, typical photoionization models calculate the ionization, excitation, and heating of cosmic gas by an external source of photons. The gas is generally assumed to be in a time-steady balance between ionization and recombination, and between heating and cooling. If the gas is optically thin, then a useful scaling parameter is the ionization parameter, defined in terms of the ratio of the incident ionizing flux to the gas density or pressure. We adopt the definition $\xi = 4\pi F/n$ where F is the incident energy flux integrated between 1 and 1000 Ry, and n is the gas number density (Tarter et al. 1969); various other definitions are also in use. When the gas is isobaric, the appropriate ionization parameter is proportional to the ratio ionizing flux/gas pressure. We adopt the combination ξ/T or $\Xi = \xi/(kTc)$ (Krolik et al. 1981) for this purpose. This much of photoionization modeling is common to today's models for X-ray sources and to more traditional models used for nebulae.

Prior to the launch of *Chandra* and *XMM-Newton*, it was recognized that objects such as AGN and X-ray binaries would have spectral features with diagnostic application when observed in the X-ray band. These included $K\alpha$ fluorescence lines from iron seen from many objects (Gottwald et al. 1995; Asai et al. 2000), and the warm absorbers in the soft X-ray band from AGN (Reynolds 1997). The quantum leap in sensitivity and spectral resolution represented by *Chandra* and *XMM-Newton* revealed that other new ingredients are needed in order to make the models useful for quantitative study of X-ray sources. This motivated a great deal of work in the treatment of physical processes previously neglected, and in the accuracy and comprehensiveness of atomic data. A summary of some of these areas will occupy the remainder of this paper.

3 Radiation Transport

Although numerical methods for radiation transfer are well established (Hubeny 2001), their implementation has the potential to be very computationally expensive. Also, radiation transfer depends sensitively on the geometrical arrangement of the gas and the sources of illuminating radiation, so it is difficult to make a calculation which has wide applicability. A calculation must treat the transfer of ionizing continuum into the photoionized gas and transfer of cooling or reprocessed radiation out of the gas. For the purposes of X-ray astronomy, it is also useful to calculate the entire synthetic spectrum produced by the photoionized plasma. This can then be used for direct fitting to data using tools such as XSPEC,¹ ISIS² or SHERPA.³

Traditional treatments of radiation transfer in photoionization models make several simplifying assumptions which allow for efficient calculation and wider applicability of model

¹<http://heasarc.gsfc.nasa.gov/docs/xanadu/xspec>.

²<http://space.mit.edu/CXC/isis>.

³<http://cxc.harvard.edu/sherpa/>.

results. These include: (i) Simplified geometry, such as a plane parallel slab or a spherical shell; (ii) Use of single-stream transport of the illuminating radiation; and (iii) Use of escape probability transport of resonance lines. We note that X-ray resonance line optical depths are typically much smaller than optical or UV line depths, so the effects of line transfer approximations are reduced compared with traditional nebular photoionization calculations.

Recent progress in radiation transfer for X-ray photoionization has centered around the application of sophisticated accurate transfer treatments for certain limited specialized problems. These include the adoption of the accelerated lambda iteration method in the Titan code (Chevallier et al. 2006; Rózańska et al. 2006; Gonçalves et al. 2007). Recently, the Monte Carlo method has been used by Sim et al. (2008, 2010) to treat the transfer in AGN broad absorption line (BAL) and warm absorber flows. This latter work combines radiation transfer with the detailed geometry derived from a numerical hydrodynamic model. It has led to important insights into the origin of spectral features such as high velocity lines, and X-ray emission lines. This work illustrates the importance of consideration of the detailed geometrical distribution of the gas, and the inherent limitations of traditional simplified geometrical assumptions.

4 Atomic Data and Comprehensiveness

The other half of the challenge of current photoionization modeling is almost entirely associated with atomic data. It has long been realized that comprehensive atomic data is crucial to accurately calculating the thermal properties of gases hotter than $\sim 10^4$ K (Kwan and Krolik 1981), and that this outweighs considerations such as the treatment of radiation transfer for traditional nebular problems. This implies consistent treatment of various ionization/excitation processes, both radiative and collisional, and their inverses, including inner shell processes, for all of the ions of the ≥ 10 most abundant elements. Similar arguments apply to the calculation of the X-ray opacity of partially ionized gases. Furthermore, the need to calculate synthetic spectra introduces a further requirement of accuracy on atomic data: observed X-ray spectra can have spectral resolution of $\varepsilon/\Delta\varepsilon \simeq 1000$, and in order to fit to such data, synthetic spectra must employ wavelengths and ionization potentials which are accurate at this level. Such precision cannot be achieved by current atomic physics calculations, and requires dedicated experiments.

A great deal of work has been done to calculate and measure atomic energy levels, cross sections and transition probabilities for the purposes of astrophysical X-ray photoionization modeling. A detailed summary would require a dedicated paper; many areas of progress have been described by Beiersdorfer (2003), Kallman and Palmeri (2007), Foster et al. (2010). Notable are the measurements carried out by the electron beam ion trap (EBIT) and storage rings in Germany and Sweden, calculations using the FAC, HULLAC, R-Matrix and Autostructure codes. Some of this work will be highlighted in the following sections.

5 Recent Topics

5.1 Iron M-shell Unresolved Transition Array (UTA)

The *Chandra* spectrum of the Seyfert 1 galaxy NGC 3783 (Kaspi et al. 2002), and spectra of similar objects, has led to significant revisions of our understanding of these sources. It has also pointed out several physical effects which were not included in previous photoionization

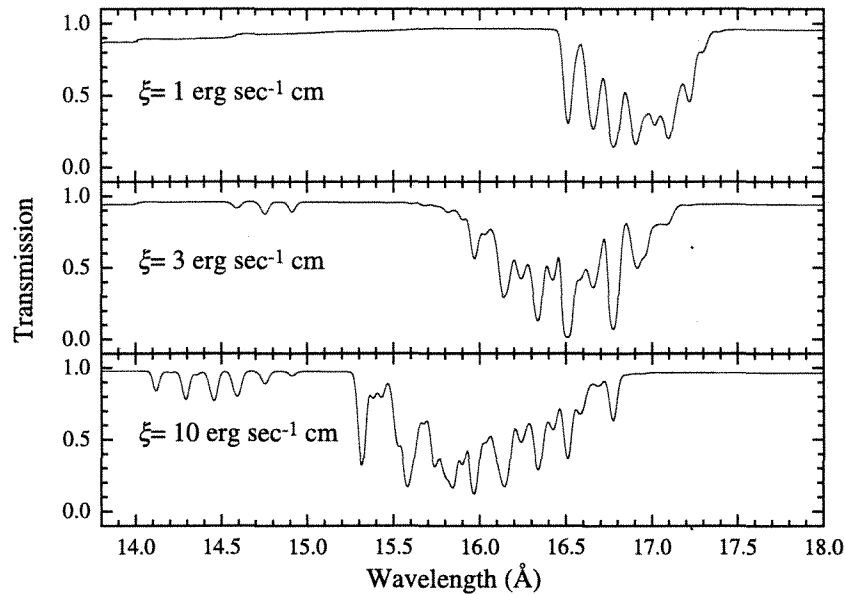


Fig. 1 Iron M shell UTA absorption for 3 different ionization parameters. From Behar et al. (2001)

models. One example is the importance of the many line features produced by transitions in iron between the levels with principle quantum numbers 2 and 3 (the L and M shells), notably from ions with 10 or more electrons, where the L shell is full. Previously these lines had only been considered in ions with partially filled L shells. Typical ions have many such lines (~ 10 – 100), grouped together in wavelength, and the ensemble is called the iron M shell unresolved transition array (UTA). The importance of these lines was first pointed out by Behar et al. (2001), who also showed that they provide an ionization diagnostic for relatively low ionization material. That is, the centroid shifts from 16–17 Å to 15–16 Å as ionization increases owing to the change from 2p–3d transitions to 2s–3p transitions as the 3p shell opens. This is illustrated in Fig. 1, taken from Behar et al. (2001).

These features are detected in most Seyfert galaxy warm absorbers, and are important diagnostics of ionization. In particular, in the case of NGC 3783, they clearly indicate the presence of low ionization iron Fe^{2+} – Fe^{8+} , and the relative absence of iron Fe^{9+} – Fe^{16+} .

5.2 Fluorescence Lines

Fluorescence lines can be emitted by gas over a wide range of ionization states. Very useful tables of the properties of these lines were provided by Kaastra and Mewe (1993). Also, it was pointed out by Palmeri et al. (2003a, 2003b) that the $K\beta/K\alpha$ ratio is a sensitive diagnostic of ionization, and this has been applied to observed spectra by Yaqoob et al. (2007) and others. Figure 2 illustrates the variety of iron K emission feature profiles and strengths that can arise for various ionization states (Kallman et al. 2004).

5.3 Resonance Scattering

In traditional nebular modeling it was typically assumed that the gas was spherically symmetric around the continuum source and stationary. If so, resonance scattering of the incident continuum is expected to have negligible effect on the spectrum seen by a distant observer.

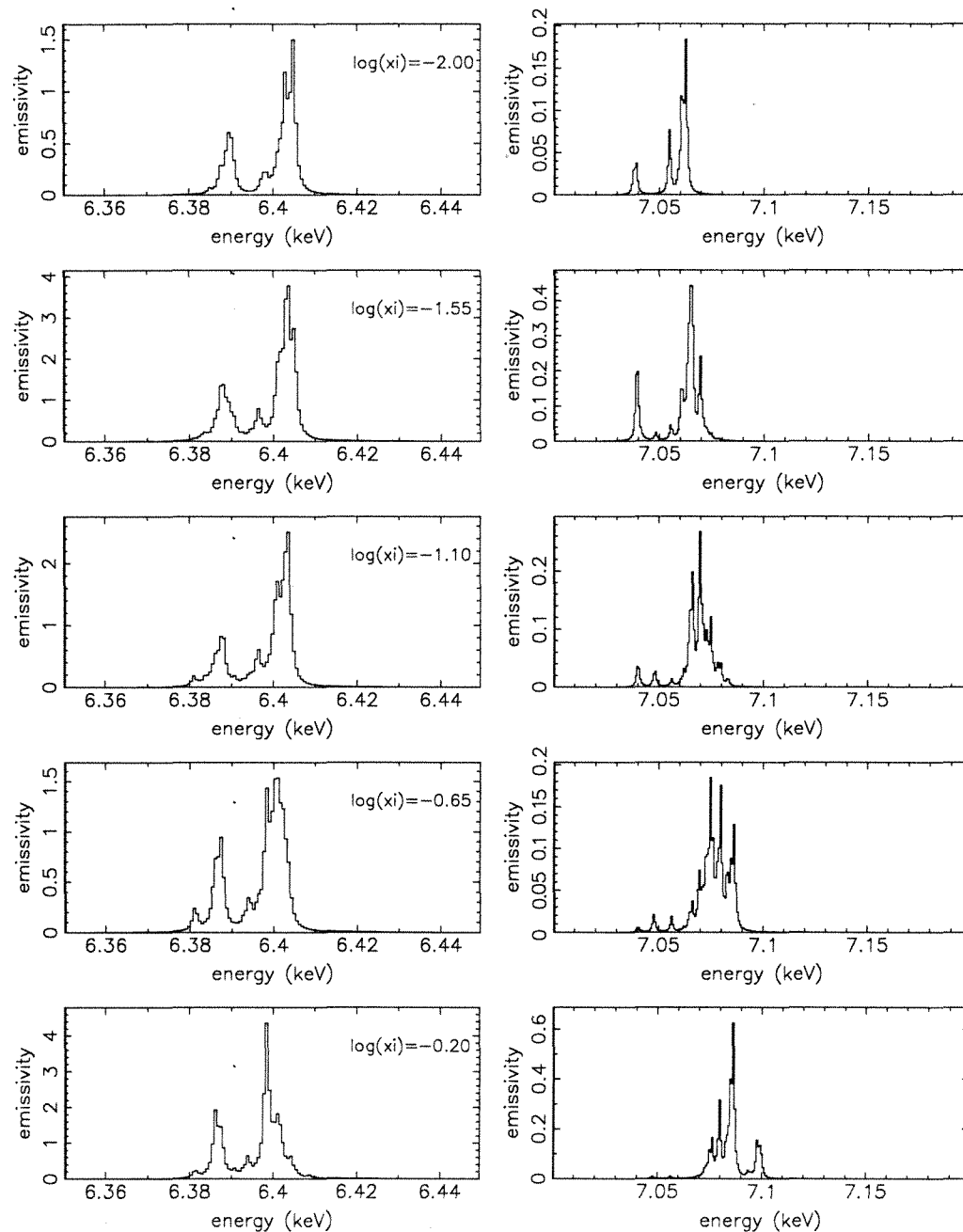


Fig. 2 Model K shell line spectra of iron for various ionization parameters (see below for definition). Emissivity units are arbitrary, but are the same for all panels. Kallman et al. (2004)

There is a cancellation between continuum photons removed from and those added to the beam of continuum we observe from the central source. In this case, the region of the spectrum emergent from the cloud which includes a resonance line would show neither a deficit nor an excess at the line energy. Of course, photoionization followed by recombination leads to a redistribution of the energy of the photons absorbed by ionization, and so would produce an excess at the line energy.

It is now recognized that many photoionization-dominated sources observed in X-rays have reprocessing gas which is not spherically distributed around the continuum source. In the case of a non-spherical scattering region, the cancellation between photons scattered out of and into the observed beam is not exact, and thus scattering can have an effect on the observed spectrum. The effect depends, crudely, on the relation between the column density between the continuum source and infinity averaged over 4π steradians, as compared with the column density along the observer's line of sight to the continuum source. If the observer's line of sight traverses more gas than the spherical-average, then resonance scattering will result in a net removal of photons from the observed radiation field and the spectrum will have a deficit at the line energy. This could be termed the 'net absorption' case. If the observer's line of sight traverses less gas than the spherical-average, then resonance scattering will result in a net addition of photons to the observed radiation field and the spectrum will have an excess at the line energy. Such apparent 'net emission' can be confused with emission due to recombination or electron impact excitation, though these can be distinguished by differing dependence on atomic quantities such as oscillator strengths or collision cross sections. Furthermore, the resonance scattering cross section is much greater than the background cross sections for photoionization, so lines are expected to saturate at column densities which are small compared to the column densities where the continuum can penetrate. Recombination emission will dominate at higher column densities and scattered emission will dominate at lower column densities. Kinkhabwala et al. (2002) have shown that resonance scattering has a distinct signature in the line ratios and line/continuum ratio in emitting plasmas. This is illustrated in Fig. 3, which shows the transition from a scattering-dominated to a recombination-dominated spectrum as a function of the column density of the plasma. The left column corresponds to what would be observed in the 'net absorption' case, and the right column corresponds to 'net emission'. At low column densities radiative pumping of resonance lines dominates because the cross sections are larger than for photoionization, and the apparent line emission in the 'net emission' case is due to resonance scattering. At high column densities the emission is dominated by recombination.

5.4 Dielectronic Recombination

It was pointed out by Netzer (2004) and Kraemer et al. (2004) that the ionization balance needed to fit the K lines of Si in the spectrum of NGC3783 was discrepant from that needed to fit the iron UTA lines. It was suggested that this was due to the use of inaccurate dielectronic recombination rates for iron, and it was postulated that the rates were larger by ~ 10 . This suggestion was confirmed, qualitatively, by Badnell (2006), who performed distorted wave calculations of the rates and obtained rate coefficients which were even greater than those suggested by Netzer (2004). Experimental confirmation was demonstrated for Fe^{13+} (Schmidt et al. 2006), and laboratory measurements have been made for ions down to Fe^{7+} (Schippers et al. 2010).

The implications of these new rates are illustrated in Figs. 4 and 5. These show the iron ionization balance and the fit of the resulting synthetic spectrum to the 800 ksec *Chandra* observation of the Seyfert 1 galaxy NGC 3783 (Kaspi et al. 2002). These are shown for two choices of dielectronic recombination rates: the new rates, adopting the fits from Badnell (2006) in the upper panels, and the rates which were previously used (these are described in Kallman and Bautista 2001; Bautista and Kallman 2001). The fits to the spectrum utilize two components of gas, each with a single ionization parameter, and both using the same velocity and line broadening. These are: $v \simeq 800$ km/s relative to the galaxy, and $v_{nrb} \simeq 300$ km/s.

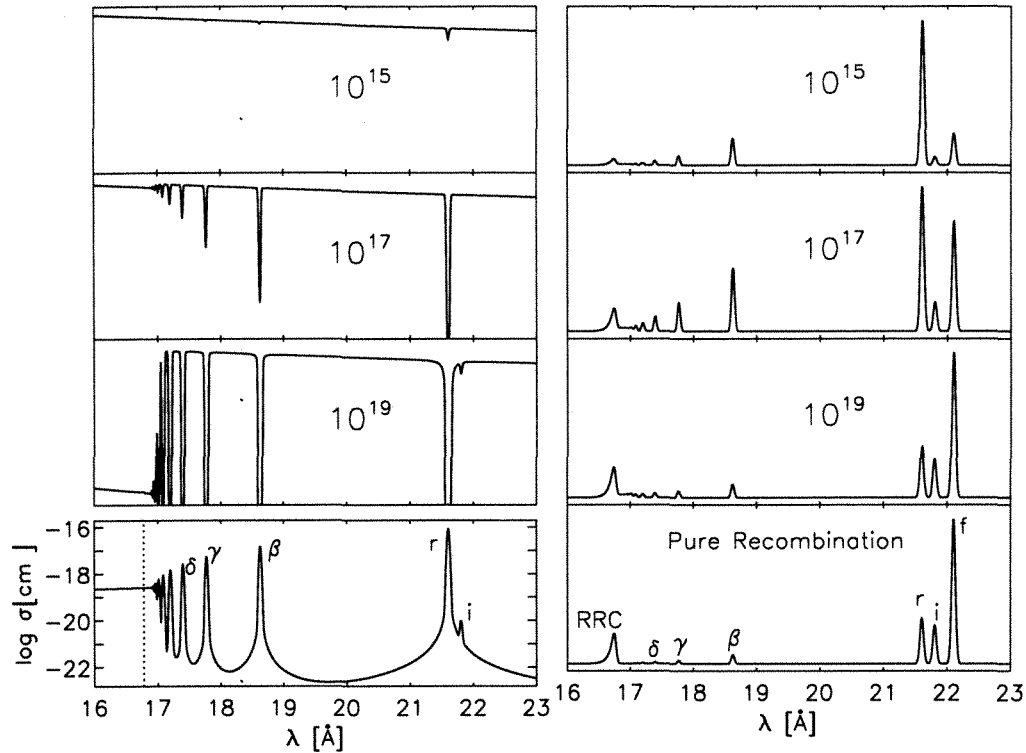


Fig. 3 Scattering-dominated spectrum from Kinkhabwala et al. (2002). *Left panel* shows spectrum seen in transmission, *right panel* shows spectrum seen in reflection

Figure 5 shows this fit using the new rates in the regions containing the iron M shell UTA and the Si K lines, showing general agreement. The ionization parameters are $\log \xi = 2$ and 1 for the new rates. The ionization balance produced by the older rates require $\log \xi = 2$ and -0.5 in order to fit the iron UTA. The Si K lines are missing from the model since the ionization state of Si is too low to allow $K\alpha$ absorption at $\log \xi = -0.5$. The fit to the model using the older rates is not shown. The older rates cannot fit the iron UTA, near 17 \AA and the Si K lines, near 7 \AA simultaneously, while the newer ones can.

5.5 Thermal Instability

A possible explanation for the two phase behavior found in the fits to the NGC 3783 spectrum is thermal instability. This is due to the properties of the cooling function in the gas which allows for two stable and one unstable solutions to the thermal equilibrium equation. This has been discussed in detail by many authors, notably in the context of quasar broad line clouds (Krolik et al. 1981; Mathews and Ferland 1987). The physical origin is the fact that the net cooling function has strong temperature dependence in some regions of temperature, and weaker dependence in other regions. This behavior is illustrated in Fig. 6, which shows surfaces of constant net cooling (defined below) in the temperature-ionization parameter plane for a photoionized gas. Here and in all the examples in this section we adopt a $\Gamma = 2$ power law for the ionizing spectrum illuminating the gas. That is, the illuminating flux is $F_e \propto \epsilon^{1-\Gamma} \text{ erg cm}^{-2} \text{ s}^{-1} \text{ erg}^{-1}$. This figure shows the equilibrium surface as a solid curve, and illustrates the difference between constant density and constant pressure gases. In the constant density case there is only a single value of equilibrium temperature for a

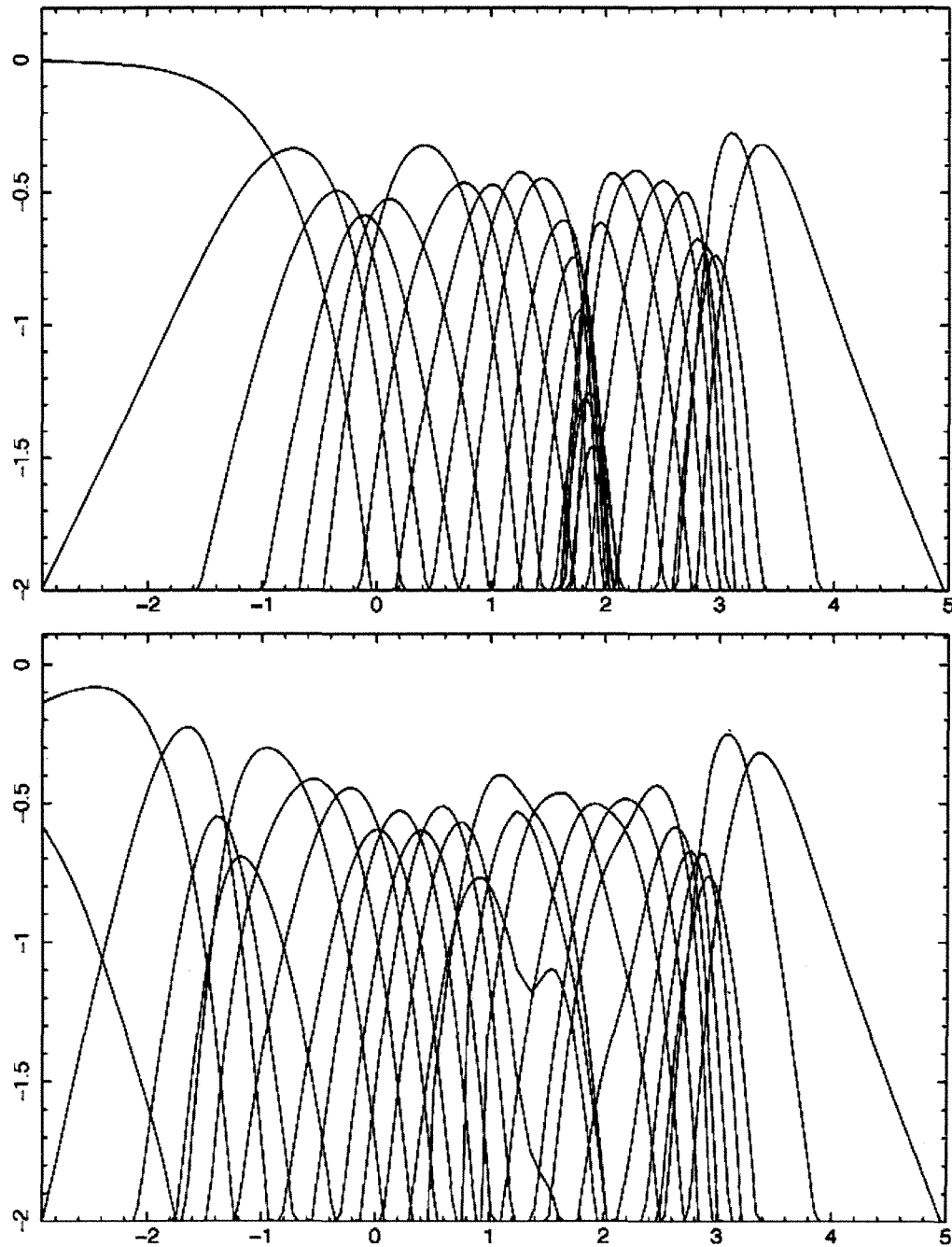


Fig. 4 Ionization balance for Fe, ion fractions on the vertical axis vs. ionization parameter. New Badnell (2006) rates for dielectronic recombination were used in the calculations shown in *upper panel*, older rates were used in the calculations shown in the *lower panel*. Vertical axis is $\log(\text{ion fraction})$ relative to the total for iron. Horizontal axis is $\log \xi$. Highest ion fraction is H-like (Fe^{25+}), corresponding to right-most curve, and lowest is neutral, corresponding to left-most curve, in both panels

given ionization parameter, while in the constant pressure case there is a narrow region of ionization parameter where three equilibria are possible.

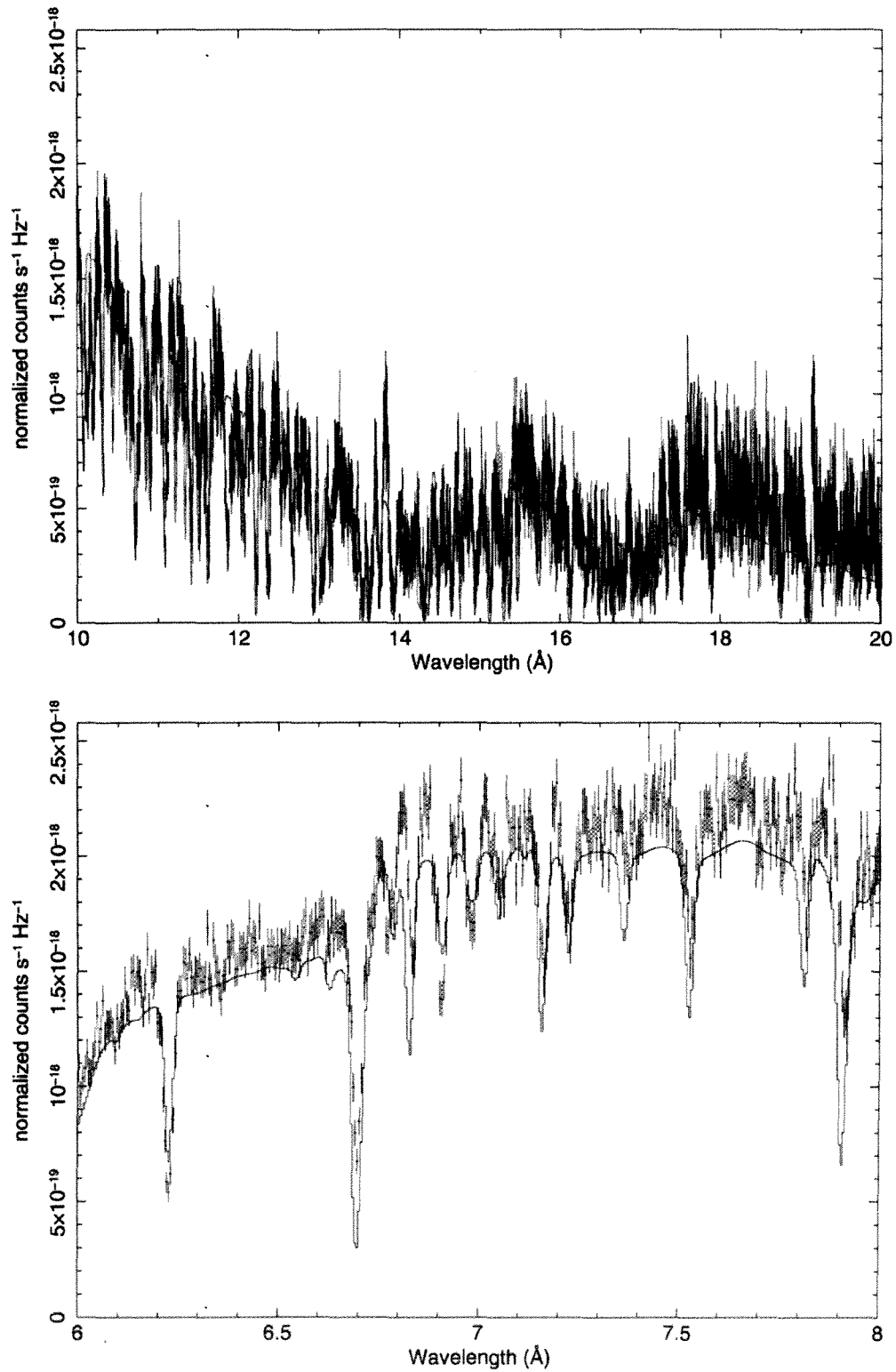


Fig. 5 Fits to the NGC3783 spectrum using Badnell (2006) rates for iron dielectronic recombination. *Upper panel:* region including the iron UTA near 17 Å. *Lower panel:* region showing the Si K lines near 6.8–7.2 Å

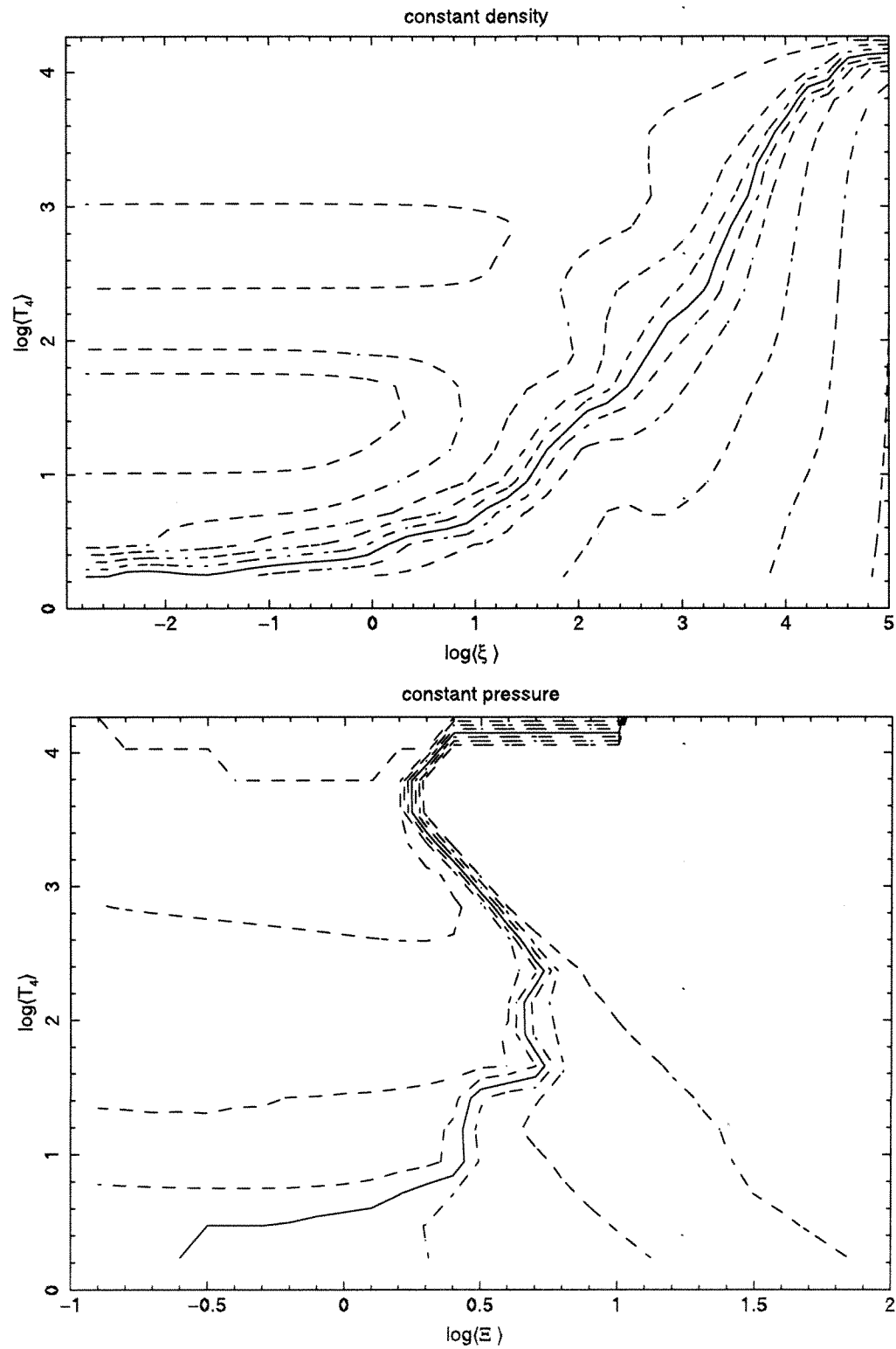


Fig. 6 Contours of constant net cooling-heating in the T - ξ plane. Upper panel: constant density; lower panel: constant pressure. Equilibrium is shown as solid curve

Thermal instability is associated with regions where the net cooling function $\Lambda(T)$ is a decreasing function of temperature. A stable temperature solution is characterized by a cooling function which is an increasing function of temperature; a positive temperature perturbation about a stable equilibrium temperature will lead to increased cooling, which will restore the gas to equilibrium, with the corresponding behavior for a negative temperature perturbation. Perturbations about an unstable temperature will tend to run away toward higher or lower temperature until a stable region of the cooling curve is reached. The net cooling function of a photoionized gas is globally increasing over the temperature range from ~ 1000 K– 10^8 K, owing to strong hydrogen cooling at low temperature, and strong inverse Compton cooling at high temperature. Instability is associated with a local maximum to the function, and so there must always be an odd number of thermal equilibrium solutions.

The instability is more likely to occur when the gas is isobaric, rather than isochoric. Isochoric gas heated by a radiation field such as that shown here, i.e. the spectral energy distribution characteristic of AGN, is predicted to be thermally stable; a radiation field which is flat, or deficient in soft photons, is more likely to produce thermal instability. The presence of the thermal instability depends on interesting things: the shape of the ionizing spectrum (SED) from IR through the X-rays, the atomic rates, elemental abundances, and (weakly) in the gas density. This suggests possible diagnostic use.

The same result is displayed in a different way in Fig. 7, which plots the heating and cooling functions per hydrogen nucleus vs. temperature for various values of the ionization parameter. The left panel shows this for constant density gas and the right panel is for constant pressure gas. In the constant density case the curves correspond to various values of the ionization parameter ξ , while in the constant pressure case the curves correspond to values of the ionization parameter Ξ . The figure shows the equilibrium solutions as colored dots: green dots correspond to solutions which are unique, i.e. values of ionization parameter for which there is only one solution; and blue dots where solutions are not unique.

The existence of thermal instability depends on the validity of the assumption of thermal (and ionization) equilibrium, and it is important to consider this when using it for quantitative work. Thermal equilibrium requires that the timescale for heating and cooling, the thermal timescale, be less than other relevant timescales. In the case of warm absorbers, which are flowing out from the AGN center, this includes the gas flow timescale.

The net cooling rate per nucleus in a photoionized gas can be written

$$L_{net} = n\Lambda - H \tag{1}$$

where Λ is the cooling rate coefficient, and the heating rate can be written:

$$H = H_X + H_C \tag{2}$$

H_X and H_C are the photoelectric and Compton heating rates, respectively, and can be written:

$$H_C \simeq n\xi\sigma_C \frac{\langle \varepsilon \rangle - 4kT}{m_e c^2} \tag{3}$$

where T is the electron kinetic temperature, $\langle \varepsilon \rangle$ is the mean photon energy, σ_C is the Compton cross section, n is the gas number density. An approximation to the photoelectric heating rate is Blondin (1994):

$$H_X \simeq 1.5 \times 10^{-21} n_{cm^3}^2 \xi^{1/4} T_K^{1/2} \left(1 - \frac{T}{T_x} \right) \text{ erg s}^{-1} \tag{4}$$

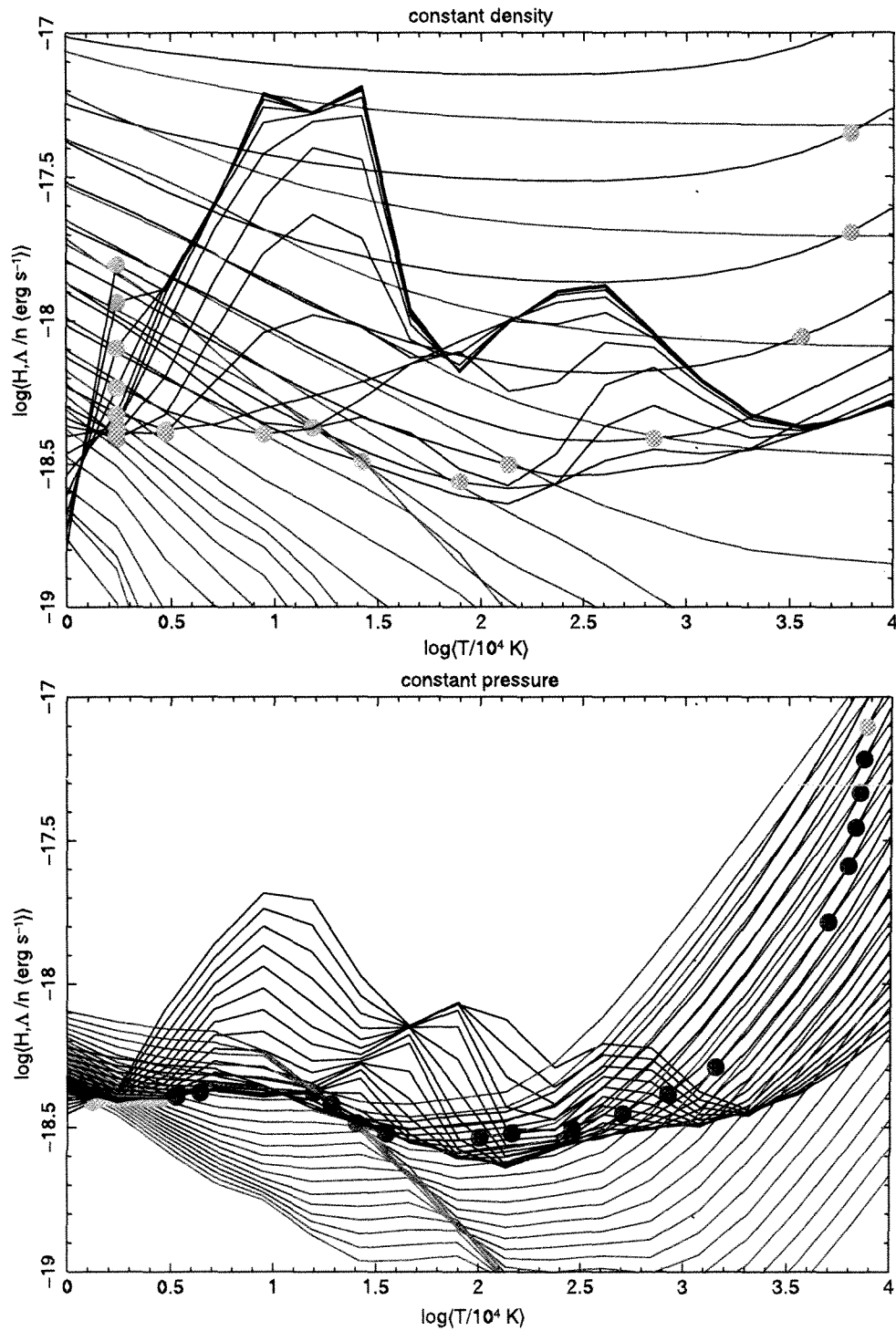


Fig. 7 Heating (red) and cooling (black) rates vs. temperature. The upper panel corresponds to constant density gas, and the curves are for values of $\log \xi$ 0–5. The lower panel corresponds to constant pressure gas and the curves are for values of $\log(\Xi)$ -1–2. Vertical axis is $\log(\text{Rate per hydrogen nucleus})$ in erg s^{-1} . Equilibrium values are shown as dots, green dots for thermally stable solutions. Blue dots correspond to equilibrium values which are either unstable, or which are stable but occur for values of Ξ which also have unstable solutions

where $T_x \simeq 10^6$ K is a typical value for power law ionizing spectra and T_K is temperature in units of K and n_{cm^3} is density in units of cm^{-3} . An approximation to the cooling rate is Blondin (1994):

$$\Lambda \simeq 3.3 \times 10^{-27} T_K^{1/2} + 1.7 \times 10^{-18} \xi^{-1} T_K^{-1/2} e^{-\frac{1.3 \times 10^5 \text{K}}{T_K}} \text{ erg cm}^3 \text{ s}^{-1} \quad (5)$$

The first term is due to bremsstrahlung and dominates at temperatures $T_x \leq T \leq T_C$. At constant pressure in this range the cooling rate per particle has temperature dependence $n\Lambda \propto T^{-1/2}$, and such gas will be thermally unstable according to the criterion of Field (1965): $dL/dT < 0$.

The cooling time is

$$t_{cool} = \frac{3kT}{L} \quad (6)$$

and using the result from (5)

$$t_{cool} \simeq 10^{16} n^{-1} T_5^{3/2} \xi_2 \text{ s} \quad (7)$$

where T_5 is the temperature in units of 10^5 K and ξ_2 is the ionization parameter in units of 10^2 erg cm^{-1} . The density n is poorly constrained, but likely values are in the range 10^4 – 10^8 . Figure 7 shows more accurate numerical calculation of these rates as a function of T and ξ . This shows the difference between constant density and constant pressure calculations, and shows the regions of thermal instability. Constant pressure is more likely to lead to thermal instability owing to the added inverse dependence of density on temperature, thereby leading to regions where the net cooling decreases with increasing temperature.

The timescale for gas to flow outward in the warm absorber is

$$t_{flow} = \frac{R}{v} \simeq 10^{11} R_{18} v_7^{-1} \text{ s} \quad (8)$$

where R is the typical flow lengthscale, R_{18} is $R/10^{18}$ cm, and v is the flow velocity. It is clear from these estimates that the timescales for cooling and flow can be comparable. Thus, the assumption of thermal equilibrium must be carefully evaluated before the thermal instability is used as a diagnostic.

Now we can test this for a more realistic model of the warm absorber. This is a 2.5 dimensional (3 dimensional axisymmetric) hydrodynamic calculation of the evaporation from the torus responsible for the obscuration in Seyfert 2 galaxies. In this model the torus is heated by a non-thermal $\Gamma = 2$ power law from the black hole. The warm absorber is formed as gas is evaporated and flows out (radiative driving is included) The thermodynamics of X-ray heating and radiative cooling is included, and the dynamics are calculated as pure hydrodynamics, no magnetohydrodynamic effects are included. The synthetic spectrum is also calculated from these simulations. These have been published in Dorodnitsyn et al. (2008); Dorodnitsyn and Kallman (2009). It is interesting to consider what happens in the T vs ξ/T plane in such a model. This is illustrated in Fig. 8, which shows the loci of T vs ξ/T for such a simulation. The effect of thermal instability is seen for temperatures near $10^{5.5}$ K, where there are fewer points.

This model shows that the thermal properties of warm absorber gas are considerably more complicated than most current models. Departures from thermal equilibrium are important. At the highest temperatures adiabatic cooling is important. This is a snapshot at one particular time in the simulation; the loci of points are not static, but are constantly moving as material is evaporated from the torus, moves outward and cools. It illustrates

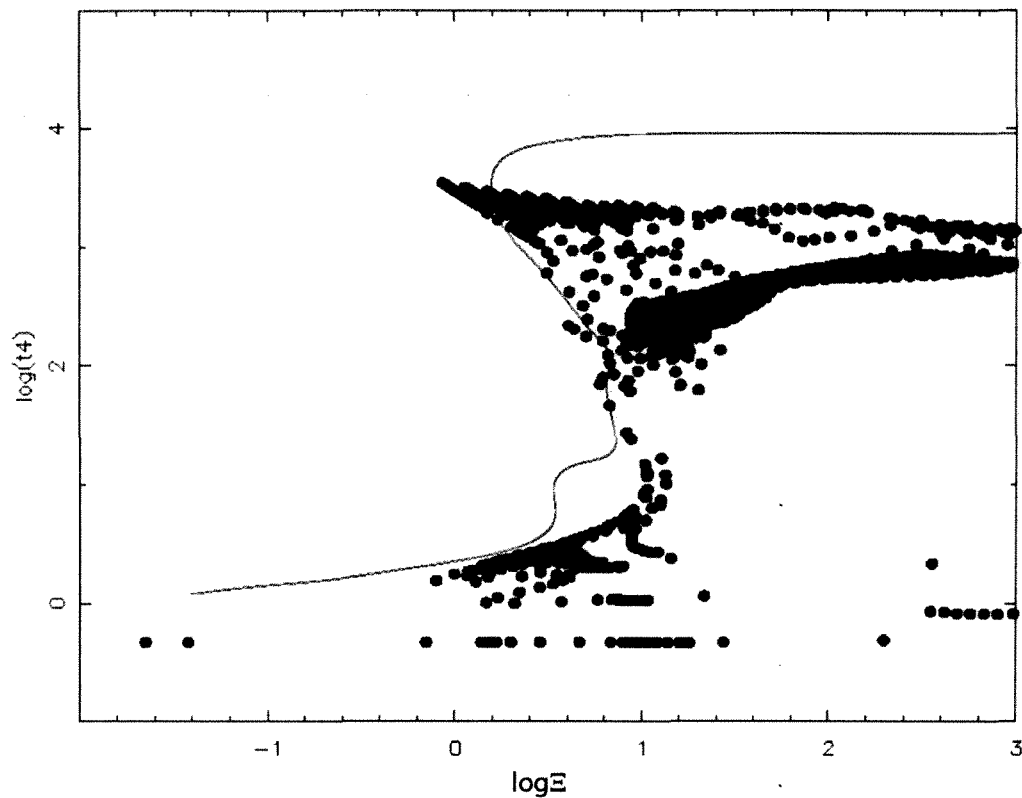


Fig. 8 Locus of points in evaporative torus hydrodynamic model. This snapshot illustrates that many zones are out of thermal equilibrium; time dependent effects are important. The thermally unstable regions are generally avoided, but not completely. Equilibrium curve is shown in *red*

that many zones are out of thermal equilibrium; time dependent effects are important. The thermally unstable regions are generally avoided, but not completely. Thus, simple stability models provide a very approximate guide for where the gas ends up. They may overestimate the ionization parameter, since non-equilibrium gas may be at a lower ionization parameter than would be inferred from fitting to equilibrium models. We should not be surprised to see gas in unstable regions. Furthermore, the appearance varies on flow timescale; the same model may look different when viewed in many different objects.

6 The Future

Fitting models of photoionized plasmas to *Chandra* and *XMM-Newton* spectra provides insights to the nature of warm absorbers and related structures: their degree of ionization, density, location, composition and kinematics. However, the models are likely still incomplete in important ways. For example, X-ray grating spectra with good statistics seldom give truly statistically acceptable fits to standard models. Typically, χ^2 per degree of freedom is ~ 2 or greater. Possible reasons include: missing lines in the atomic database, incorrect treatment of line broadening, incorrect ionization balance, overly idealized assumptions (such as ionization equilibrium), inaccurate treatments of radiative transfer or geometrical effects. In addition to thinking about these things, modelers need to prepare for the next generation of

X-ray instruments, which will likely have improved sensitivity in the iron K energy band. This will allow quantitative study of lines from trace elements such as Cr and Mn. Another frontier is low ionization material; these instruments may detect inner shell fluorescence from many elements with $Z > 10$. Time dependent effects deserve more exploration, as do more user friendly general purpose radiative transfer models. Photoionization modelers will be helped by laboratory measurements and atomic theory if this results in more accurate and comprehensive line wavelengths. The quest for good fits also depends on accurate instrumental calibration, including the response to narrow features, and accurate calibration of continuum for accurate subtraction. Users of photoionization models can provide feedback to modelers and others in order to detect errors and improve the user interface.

Acknowledgements I thank Dr. Ehud Behar and Dr. Daniel Savin for constructive comments, and my collaborators: M. Bautista, A. Dorodnitsyn, J. Garcia, C. Mendoza, P. Palmeri, P. Quinet, and M. Witthoef.

References

- K. Asai, T. Dotani, F. Nagase, K. Mitsuda, *Astrophys. J. Suppl.* **131**, 571 (2000)
 N.R. Badnell, *Astrophys. J. Lett.* **651**, L73 (2006)
 M. Bautista, T. Kallman, *Astrophys. J. Suppl. Ser.* **134**, 139 (2001)
 E. Behar, M. Sako, S.M. Kahn, *Astrophys. J.* **563**, 497 (2001)
 P. Beiersdorfer, *Annu. Rev. Astron. Astrophys.* **41**, 343 (2003)
 J.M. Blondin, *Astrophys. J.* **435**, 756 (1994)
 A. Burgess, M.J. Seaton, *Mon. Not. R. Astron. Soc.* **120**, 121 (1960)
 L. Chevallier, S. Collin, A.-M. Dumont, B. Czerny, M. Mouchet, A.C. Gonçalves, R. Goosmann, *Astron. Astrophys.* **449**, 493 (2006)
 A. Dorodnitsyn, T. Kallman, *Astrophys. J.* **703**, 1797 (2009)
 A. Dorodnitsyn, T. Kallman, D. Proga, *Astrophys. J.* **687**, 97 (2008)
 G.B. Field, *Astrophys. J.* **142**, 531 (1965)
 A.R. Foster, R.K. Smith, N.S. Brickhouse, T.R. Kallman, M.C. Witthoef, *Space Sci. Rev.* (2010, this issue)
 A.C. Gonçalves, S. Collin, A.-M. Dumont, L. Chevallier, *Astron. Astrophys.* **465**, 9 (2007)
 M. Gottwald, A.N. Parmar, A.P. Reynolds, N.E. White, A. Peacock, B.G. Taylor, *Astron. Astrophys. Suppl. Ser.* **109**, 9 (1995)
 I. Hubeny, *Spectrosc. Chall. Photoion. Plasmas* **247**, 197 (2001)
 J.S. Kaastra, R. Mewe, *Astron. Astrophys. Suppl. Ser.* **97**, 443 (1993)
 T.R. Kallman, *Spectrosc. Chall. Photoion. Plasmas* **247**, 175 (2001)
 T.R. Kallman, M. Bautista, *Astrophys. J. Suppl. Ser.* **133**, 221 (2001)
 T.R. Kallman, P. Palmeri, *Rev. Mod. Phys.* **79**, 79 (2007)
 T.R. Kallman, P. Palmeri, M.A. Bautista, C. Mendoza, J.H. Krolik, *Astrophys. J. Suppl. Ser.* **155**, 675 (2004)
 S. Kaspi et al., *Astrophys. J.* **574**, 643 (2002)
 A. Kinkhabwala et al., *Astrophys. J.* **575**, 732 (2002)
 S.B. Kraemer, G.J. Ferland, J.R. Gabel, *Astrophys. J.* **604**, 556 (2004)
 J.H. Krolik, C.F. McKee, C.B. Tarter, *Astrophys. J.* **249**, 422 (1981)
 J. Kwan, J.H. Krolik, *Astrophys. J.* **250**, 478 (1981)
 W.G. Mathews, G.J. Ferland, *Astrophys. J.* **323**, 456 (1987)
 H. Netzer, *Astrophys. J.* **604**, 551 (2004)
 D.E. Osterbrock, G.J. Ferland, in *Astrophysics of gaseous nebulae and active galactic nuclei*, 2nd edn., ed. by D.E. Osterbrock, G.J. Ferland (University Science Books, Sausalito, 2006)
 P. Palmeri, C. Mendoza, T.R. Kallman, M.A. Bautista, M. Meléndez, *Astron. Astrophys.* **410**, 359 (2003a)
 P. Palmeri, C. Mendoza, T.R. Kallman, M.A. Bautista, *Astron. Astrophys.* **403**, 1175 (2003b)
 C.S. Reynolds, *Mon. Not. R. Astron. Soc.* **286**, 5 (1997)
 A. Różańska, R. Goosmann, A.-M. Dumont, B. Czerny, *Astron. Astrophys.* **452**, 1 (2006)
 S. Schippers, M. Lestinsky, A. Müller, D.W. Savin, E.W. Schmidt, A. Wolf (2010). arXiv:1002.3678
 E.W. Schmidt et al., *Astrophys. J. Lett.* **641**, L157 (2006)
 M.J. Seaton, *Mon. Not. R. Astron. Soc.* **118**, 504 (1958)
 M.J. Seaton, *Mon. Not. R. Astron. Soc.* **119**, 81 (1959)
 S.A. Sim, K.S. Long, L. Miller, T.J. Turner, *Mon. Not. R. Astron. Soc.* **388**, 611 (2008)
 S.A. Sim, D. Proga, L. Miller, K.S. Long, T.J. Turner, (2010). arXiv:1006.3449
 C.B. Tarter, W.H. Tucker, E.E. Salpeter, *Astrophys. J.* **156**, 943 (1969)
 T. Yaqoob et al., *Publ. Astron. Soc. Jpn.* **59**, 283 (2007)
 H. Zanstra, *Astrophys. J.* **65**, 50 (1927)

